THE JOURNAL OF PHYSICAL CHEMISTRY B

Article

pubs.acs.org/JPCB

Importance of Molecular Structure on the Thermophoresis of Binary Mixtures

Pardeep Kumar and Debabrata Goswami*

Department of Chemistry, Indian Institute of Technology Kanpur, Kanpur, Uttar Pradesh 208016, India

ABSTRACT: Using thermal lens spectroscopy, we study the role of molecular structural isomers of butanol on the thermophoresis (or Soret effect) of binary mixtures of methanol in butanol. In this study, we show that the thermal lens signal due to the Soret effect changes its sign for all the different concentrations of binary mixtures of butanol with methanol except for the one containing *tertiary*-butanol. The magnitude and sign of the Soret coefficients strongly depend on the molecular structure of the isomers of butanol in the binary mixture with methanol. This isomerization dependence is in stark contrast to the expected mass dependence of the Soret effect.

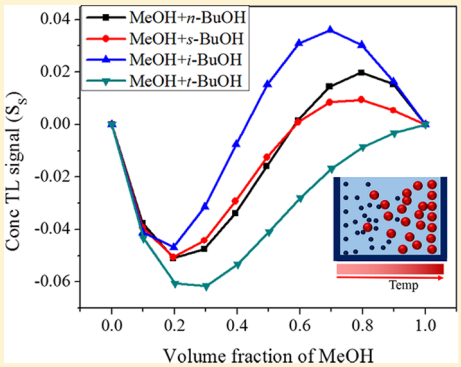

INTRODUCTION

Thermophoresis is a physical phenomenon of concentration gradient arising in a mixture of two or more components when it is exposed to a thermal gradient. This was first observed by Ludwig[1] in 1856. Later in 1879, it was studied in great detail by Charles Soret.[2] So, this phenomenon is also called the Ludwig–Soret effect, though more commonly it is known as the Soret effect. As a result of this phenomenon, under the influence of a thermal gradient, relative thermal diffusion of the components of the mixture occur, resulting in separation of components. However, when this process starts, the Fickian diffusion process starts in the opposite direction[3] to equilibrate the concentration gradient. Then net flux is given as[3]

$$J = -\rho(D\nabla c + D_T c(1 - c)\nabla T) \quad (1)$$

where, ρ (kg/m^3) is the density of the binary mixture, D (m^2/s) is the molecular diffusion coefficient, c is the mass fraction of the reference species, D_T (m^2/s K) is the thermal diffusion coefficient, and T is the temperature in Kelvin. When the net flux is zero, $\nabla_c = S_T c(1 - c)\nabla T$, where $S_T = D_T/D$ is the Soret coefficient with unit K^{-1}. It has a positive value when the heavier component migrates to the cold side and a negative value otherwise. Many authors also show that the change of sign of the Soret coefficient takes place with compositions.[4,5] The Soret effect has a wide range of applications in characterization and separation of polymers[6,7] and isotopes separation.[8,9] It is also extensively used for studying various biological processes.[10−12] A lot of work has been done on the Soret effect for understanding the phenomenon and its applications.[13−19] Since this concentration gradient (Soret effect) is generated in the millimeter to micrometer range, the thermal lens (TL) spectroscopy becomes a great tool to study this effect.[20−26]

TL is a result of temperature change arising from the nonradiative relaxation in the system being irradiated by a laser beam.[27−29] This temperature change results in a refractive index change in the system. This refractive change is in the form of a smooth gradient in the case of the Gaussian laser beam profile. This refractive index gradient makes the system behave as a lens. TL can be either a diverging lens or a converging lens, depending on the thermo-optic coefficient (dn/dT)[30] of the system under study. The wavelength of the laser beam is chosen in such a manner that couples with either the electronic levels or the vibrational levels of the sample under study. The TL process starts with the absorption of the laser beam and continues until the system reaches thermal equilibrium. The amount of heat deposited in the system depends on the amount of radiationless relaxation. Presently, TL spectroscopy is a well-known, highly sensitive, nondestructive, popular analytical technique[31−39] for the thermal, optical, and chemical analysis of solids, liquids, and gases.[40−44]

In 1965, Gordon et al.[45] observed that a laser beam diverges after passing through a nearly transparent solvent. This divergence of the laser beam could only be explained if there is a decrease in the refractive index of the sample due to heat deposition in the system. This observation led to TL spectroscopy using a single laser beam.[46] To enhance the sensitivity of the TL spectroscopy, the dual-beam TL technique has been developed.[47,48] The dual-beam TL technique is more sensitive compared to the single-beam TL technique, as in the dual-beam case, one beam creates the TL signal while the second beam measures this TL signal. A more accurate signal measurement can be done in this case compared to the single-

Received: August 6, 2014
Revised: November 22, 2014
Published: November 24, 2014

dx.doi.org/10.1021/jp5079604 | J. Phys. Chem. B 2014, 118, 14852−14859

beam TL technique. This dual beam TL technique has two types of experimental setups, namely, the mode-matched and the mode-mismatched, depending on the beam waist parameters of the pump and the probe beams.[48] The mode-mismatched TL technique is more sensitive compared to the mode-matched TL technique, and is used widely for photochemical study[49−51] and hydrodynamic relaxation to measure the Soret effect.[20−26] Continuous wave (cw) lasers are typically used in TL study, but, recently, femtosecond high repetition rate (HRR) lasers are also being used for TL study. Each femtosecond pulse deposits a small amount of energy to the sample and, in the case of the HRR laser, this small amount of energy accumulates to result in a long time TL signal. The HRR laser provides better signal-to-noise ratio compared to the cw laser.[52]

The Soret effect depends on the difference in the masses of the components of a mixture. Thus, most of the work on the Soret effect was performed on mixtures containing components of different masses.[6−26] Only a very limited study of the effect of molecular structure of the components of a mixture on the Soret effect is available,[53] and a systematic study is yet to be done. We explore the molecular structure effect on the Soret phenomenon systematically. For such a study, we used the structural isomers of butanol: normal-butanol (*n*-BuOH), secondary-butanol (*sec*-BuOH), iso-butanol (i-BuOH), and tertiary-butanol (*t*-BuOH); and prepared their individual binary mixtures with the constant second component as methanol (MeOH).

EXPERIMENT

The experimental setup used for studying the molecular structure effect on the Soret phenomenon is a two-color pump−probe mode-mismatched TL technique as shown in Figure 1. The experimental setup comprises a mode-locked Er-doped femtosecond fiber laser (Femtolite Mira, Inc.). This laser produces laser pulses of two colors centered at 1560 and 780 nm with a repetition rate of 50 MHz. The laser pulses centered at 1560 nm has the pulse width of ∼300 fs with an average power of 12 mW at the sample, while the laser beam of pulses centered at 780 nm has the pulse-width of ∼100 fs with an average power of 6 mW at the sample. The laser beam of pulses centered at 1560 nm acts as the pump pulse and is focused on the sample. The laser beam of pulses centered at 780 nm acts as the probe beam and is collimated through the sample with the telescopic arrangement of two lenses (Figure 1). To measure the position-dependent TL signal, a motorized translational stage (Newport: M-6 UTM150CC.1) is used to scan the sample across the focal point of the pump beam (Figure 2).

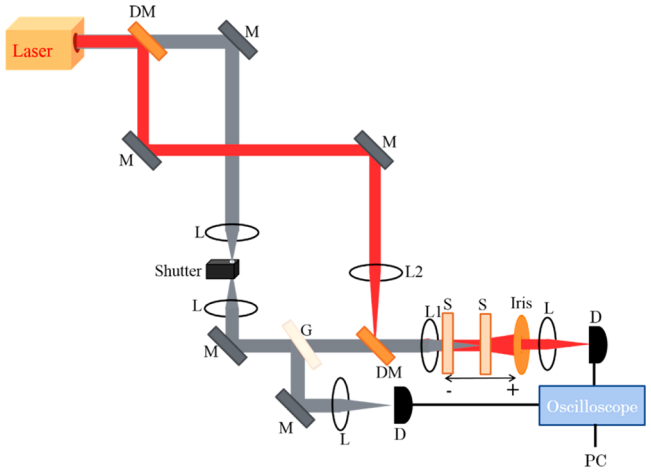

Figure 1. Schematic diagram of experimental setup: (DM) dichroic mirror; (M) mirror; (L) lens; (G) glass plate; (S) sample; (D) detector; (PC) personal computer.

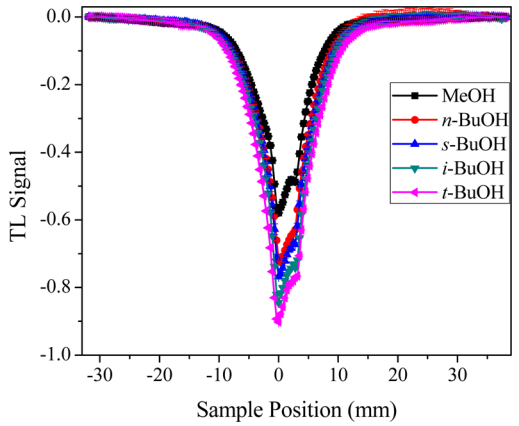

Figure 2. TL signals for pure samples, namely, MeOH, *n*-BuOH, *s*-BuOH, *i*-BuOH, and *t*-BuOH, with respect to the Z-position of the sample.

The sample cell used has a width of 1 mm. The strength of the TL signal is measured by measuring the transmittance of the probe beam through a 60% closed aperture situated in the far field. The intensity of the probe beam is measured with the help of an amplified silicon photodetector (Thorlabs: PDA 100A-EC) with a 200 MHz oscilloscope (Tektronix TDS 224). A National Instruments GPIB card is used to interface the oscilloscope to the computer. A LabVIEW code is written for data acquisition. An InGaAs photodiode (Acton Research) (Figure 1) is used to measure the absorption of the pump beam by the sample. The same photodiode also used to analyze the fluctuation in the pump beam. The maximum TL signal is found at the focal point of the pump beam. For analysis of hydrodynamics relaxation, a shutter is used in the pump beam, and the sample is placed at the focal point of the pump beam. A telescopic arrangement is used to reduce the activation time of the shutter (Figure 1).

The samples used in this study (*n*-BuOH, *s*-BuOH, *i*-BuOH, *t*-BuOH, and MeOH) are of spectroscopy grade and were purchased from Sigma-Aldrich India. The binary mixtures are prepared by adding MeOH to the respected isomer of butanol (MeOH + *n*-BuOH, MeOH + *s*-BuOH, MeOH + *i*-BuOH, MeOH + *t*-BuOH) volumetrically.

RESULT AND DISCUSSION

The alcohols have strong absorption in the communication band due to hydroxyl group (OH). This absorbed energy is transformed to heat via nonradiative relaxation. This heat generated in the sample results in a TL. The strength of the TL signal is measured by observing the change in the probe beam divergence. The change in probe beam intensity through a closed aperture located in the far field is an indirect way of measuring the probe beam divergence. The magnitude of stationary TL signal at different sample positions with respect to the focal point of the pump beam is measured by the relation

dx.doi.org/10.1021/jp5079604 | J. Phys. Chem. B 2014, 118, 14852−14859

$$S(z, t_\infty) = \frac{I(z, t_\infty) - I_0}{I_0} \quad (2)$$

where, $S(z, t_\infty)$, is the strength of stationary TL signal at each Z-position of the pure samples (Figure 2). $I(z, t_\infty)$ and I_0 are the probe beam transmittance through the aperture in the presence of the pump beam after a sufficiently long time and in the absence of the pump beam, respectively. The maximum TL signal is observed at the focal point of the pump beam through the pump−probe mode-mismatched TL technique. This can be seen in Figure 2. A comparison of TL signal with absorption of the pump beam by the sample is presented in Figure 3.

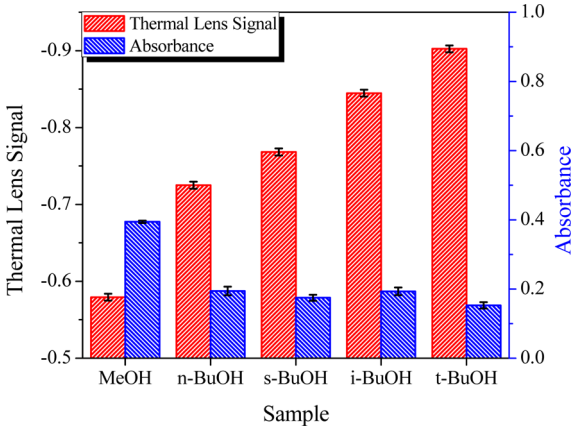

Figure 3. TL signals for pure samples at the focal point of pump beam ($z = 0$) relative to the absorbance of the probe beam by the samples.

Despite the fact that methanol has a strong absorption of the pump beam, it has a small TL signal in comparison to the isomers of butanol. The magnitude of TL signal for pure samples, in the case of a strongly absorbing sample, depends on a number of factors that include:whether the absorbed energy is transferred by conduction and/or convection, absorption coefficient (α), thermal conductivity (k), thermal expansion coefficient (β), thermo-optic coefficient (dn/dT), heat capacity (c_p), etc. Our previous work has shown that the widely used model for TL[47] can be modified to the following form for highly absorbing samples:[54,55]

$$\frac{I(t)}{I(0)} = \left[1 - \frac{(\theta_1 + \theta_2)}{2}\tan^{-1}\left\{\frac{2mv}{\left(\frac{((1+2m)^2 + v^2)t_c}{2t}\right) + 1 + 2m + v^2}\right\}\right]^2 + F\left[\frac{(\theta_1 + \theta_2)}{4}\ln\left(\frac{[1 + 2m/(1 + 2t/t_c)]^2 + v^2}{(1 + 2m)^2 + v^2}\right)\right]^2 \quad (3)$$

This model is based on the fact that the absorbed heat energy has two modes of heat transfer: one is heat conduction, and the other is heat convection. As α is the absorption coefficient and P_e is the power of the pump laser beam, the amount of heat absorbed is αP_e. The part of the energy transferred by conduction is "A" while the rest of energy "$(\alpha P_e - A)$" is transferred by convection. The symbols used in the above eq 3 are defined as $\theta_1 = -A(dn/dT)/\lambda_p k$, and $\theta_2 = -((\alpha P_e - A)\, l(dn/dT)\exp(-t/t_d) = \theta_{conv}\exp(-t/t_d)$, where P_e is the power of the pump beam, λ_p is the probe beam wavelength, α is the absorption coefficient, dn/dT is the thermo-optic coefficient, k is the thermal conductivity, and t_c $(= \omega_e^2 \rho c/4k)$ is the characteristic time constant of the sample. The h is the capability of the system to transfer heat by convection. The magnitude of h depends upon a number of factors, such as molecular structure, temperature, type of heat source, etc., and t_d is defined as the time constant for the heat convection. In this particular study, the sample is put at the focal point of the pump beam, viz., 1560 nm beam. The parameters 'm' and 'v' are the experimental parameters defined as $m = (\omega_p/\omega_e)^2$, where ω_p and ω_e are the beam waists of the probe and the pump at the focal point of the pump beam, respectively; and $v = z/z_p$, where z is the distance of the sample from the beam waist position of probe beam, and z_p is the Rayleigh range of probe beam. Figure 4 (inset) shows the experimental parameters used

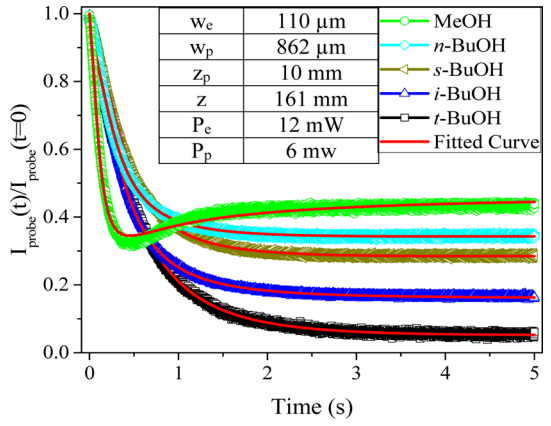

Figure 4. Time-resolved signals for the pure samples, namely, MeOH, *n*-BuOH, *s*-BuOH, *i*-BuOH, and *t*-BuOH fitted to the model described in text. The experimental parameters of the pump and probe beams are shown in the inset.

in this study as well as the pump and probe beam parameters measured at the focal point of the pump beam. The physical parameters of the pure samples are given in Table 1. The model

Table 1. Sample Parameters Used to Fit the Model Described in Eq 3

sample	thermal conductivity (k) (W m^{-1} K^{-1})	thermo-optic coefficient (dn/dT) (K^{-1}) x 10^4	absorbance
n-BuOH	0.15[a]	−4.11[b]	0.194
s-BuOH	0.13[a]	−4.41[c]	0.175
i-BuOH	0.13[a]	−3.67[d]	0.193
t-BuOH	0.12[a]	−5.63[c]	0.153
MeOH	0.2[b]	−3.98[b]	0.394

[a]From ref 56. [b]From ref 57. [c]From ref 58. [d]From ref 59.

described in eq 3 is fitted with the experimental data measured with the help of shutter by placing the sample at the focal point of the pump beam (Figure 4). The fitted parameters are shown in Table 2, wherefrom it is evident that these samples behave distinctly from each other. For example, methanol has the shortest convective time constant and the largest value of h in comparison to the rest of the samples. The isomers of butanol also behave differently under the thermal gradient, which is evident from Table 2 as the molecular structure has a strong effect on molecular diffusion.[54] It is found that among the isomers of BuOH, the convection time constant (t_d) is smallest for *n*-BuOH and the highest for *t*-BuOH. The molecular branching makes the system sluggish and corresponding molecular drift becomes progressively difficult as in the case of *t*-BuOH.

dx.doi.org/10.1021/jp5079604 | J. Phys. Chem. B 2014, 118, 14852−14859

Table 2. Fitted Parameters for the Model Described in Eq 3

sample	θ_1	θ_{conv}	h (w/m k)	F	t_c (ms)	t_d (ms)	expected t_c (ms)	χ^2
MeOH	0.57	1.10	2.09	0.15	33	124	30.38	0.97
n-BuOH	0.35	0.81	1.45	0.22	40	457	38.28	0.99
s-BuOH	0.28	0.98	1.17	0.17	47	549	48.49	0.99
i-BuOH	0.29	1.05	1.00	0.08	43	463	44.96	0.99
t-BuOH	0.50	1.08	1.16	0.02	57	856	61.06	0.99

As mentioned previously, the Soret effect mainly depends on the masses of components of a mixture exposed to a thermal gradient. The molecular mass of methanol is different from butanol, while all the isomers of butanol have the same molecular mass. So we prepared the binary mixtures of methanol with each isomer of butanol and successively changed the relative composition of the two components in each binary mixture to study molecular structure effect on the Soret phenomenon. Cabrera et al.[24,26,42] substantiated the contribution of the TL signal due to Soret effect (S_S) to the total TL signal (S_{Total}) measured experimentally as follows:

$$S_{Total}(z, t) = S_{Th}(z, t) - S_S(z, t) \tag{4}$$

where S_{Th} is the TL generated due to the temperature gradient in the system. In the same spirit, we modify eq 3 after including the Soret contribution in the following manner:

$$S_{total}(z, t) = \left[1 - \frac{(\theta_1 + \theta_2 - \theta_s)}{2} \tan^{-1}\left\{\frac{2mv}{\left(\frac{((1+2m)^2+v^2)t_c}{2t}\right) + 1 + 2m + v^2}\right\}\right]^2 + F\left[\frac{(\theta_1 + \theta_2 - \theta_s)}{4} \ln\left(\frac{\left[1 + \frac{2m}{(1+2t/t_c)}\right]^2 + v^2}{(1+2m)^2 + v^2}\right)\right]^2 - 1 \tag{5}$$

All the parameters are same as previously defined in eq 3, except the parameter θ_s, which is the contribution of the Soret effect to the TL signal as defined by Cabrera et al.[24,26,42] We modify the form of θ_s considering conduction and convection as follows:

$$\theta_s = \frac{S_T c(1-c) l \, dn/dc}{\lambda_p}\left(\frac{A}{k} + \frac{(\alpha P_e - A)}{h}\right) \times \left[1 - \sum_{i=1}^{\infty} \frac{4}{(2i-1)\pi} \sin\left[\frac{(2i-1)\pi}{2}\right] \exp\left[-(2i-1)^2 \frac{t}{t_s(z)}\right]\right] \tag{6}$$

$$\theta_s = \theta_c\left[1 - \sum_{i=1}^{\infty} \frac{4}{(2i-1)\pi} \sin\left[\frac{(2i-1)\pi}{2}\right] \exp\left[-(2i-1)^2 \frac{t}{t_s(z)}\right]\right] \tag{7}$$

where, S_T is the Soret coefficient and t_s is time constant for the development of concentration gradient, c is the concentration of the reference compound, θ_c is the phase change due to the concentration gradient. The rest of the parameters are already defined in eq 3. The total signal for the stationary TL ($t \to \infty$) is given at the focal point of the pump beam as

$$S_{total}(z, t_\infty) = \left[1 - \frac{(\theta_1 + \theta_{conv} - \theta_c)}{2} \tan^{-1}\left\{\frac{2mv}{1 + 2m + v^2}\right\}\right]^2 + F\left[\frac{(\theta_1 + \theta_{conv} - \theta_c)}{4} \ln\left(\frac{1 + v^2}{(1+2m)^2 + v^2}\right)\right]^2 - 1 \tag{8}$$

The stationary TL signal is measured at the focal point of the pump beam by scanning the samples across the focal point while each data point is taken after 5 s, so that a stationary TL formed for every data point. Equation 8 describes the relation between the total stationary TL signal arising from the contribution of the thermal gradient and the concentration gradient (Soret mechanism). The contribution of the Soret effect to the total stationary TL signal is deduced by subtracting the contribution of temperature gradient TL signal from the total stationary TL signal. Equation 8 can be further simplified for deducing the contribution of TL signal for a concentration gradient. Since θ_c contribution to the TL signal is very small, the second order term in eq 8 can be easily be neglected to arrive at the following form for the TL signal due to Soret effect:

$$S_s(z_0, t_\infty) = S_{Total}(z, t_\infty) + (\theta_1 + \theta_{conv})X \tag{9}$$

which can be rewritten as

$$\theta_c = \frac{S_{Total}(z, t_\infty) + (\theta_1 + \theta_{conv})X}{2X + \tan^{-1}(2mv/(1 + 2m + v^2))} \tag{10}$$

where

$$X = \tan^{-1}\left(\frac{2mv}{1 + 2m + v^2}\right) - (\theta_1 + \theta_{conv}) \times \left(\frac{1}{4}\left(\tan^{-1}\left(\frac{2mv}{1 + 2m + v^2}\right)\right)^2 + \frac{F}{16}\left(\ln\left(\frac{1 + v^2}{(1+2m)^2 + v^2}\right)\right)^2\right) \tag{11}$$

$$\theta_1 = -A(dn/dT)/\lambda_p k \tag{12}$$

$$\theta_{conv} = -((\alpha P_e - A) l (dn/dT)/\lambda_p h) \tag{13}$$

All the necessary parameters for the Soret effect (eq 10) can be calculated from the experimental and physical parameters of the binary mixtures in steady state conditions as is evident from eqs 11−13. The physical parameters (k, β, dn/dT, c_p, h) for the binary mixtures are calculated in the following manner. The molecular interactions between the two components of the binary mixture are taken as ideal since both of the components are organic solvents and they are both alcohols. The refractive index of binary mixtures can be represented using the Lorentz−Lorentz equation as[28,40]

$$\left(\frac{n^2 - 1}{n^2 + 2}\right)\frac{1}{\rho} = \left(\frac{n_1^2 - 1}{n_1^2 + 2}\right)\frac{x_1}{\rho_1} + \left(\frac{n_2^2 - 1}{n_2^2 + 2}\right)\frac{x_2}{\rho_2} \tag{14}$$

dx.doi.org/10.1021/jp5079604 | J. Phys. Chem. B 2014, 118, 14852−14859

After some manipulation, the refractive index of the sample can be given by the following equation:

$$n = \left(\frac{2L + 1}{1 - L}\right)^{1/2} \tag{15}$$

where

$$L = \left[\left(\frac{n_1^2 - 1}{n_1^2 + 2}\right)\frac{x_1}{\rho_1} + \left(\frac{n_2^2 - 1}{n_2^2 + 2}\right)\frac{x_2}{\rho_2}\right]\rho \tag{16}$$

The parameters k, β, ρ, A, h, F, and Abs for binary liquid mixtures are calculated in the following equations:

$$k = k_1 + (k_2 - k_1)x_2$$
$$h = h_1 + (h_2 - h_1)x_2$$
$$F = F_1 + (F_2 - F_1)x_2$$
$$\rho = \rho_1 + (\rho_2 - \rho_1)v_{x2}$$
$$\beta = \beta_1 + (\beta_2 - \beta_1)v_{x2}$$
$$A = A_1 + (A_2 - A_1)v_{x2}$$
$$\text{Abs} = l\sum_{i=1,2}\varepsilon_i c_i \tag{17}$$

Indices 1 and 2 refer to the components of the binary mixture. The v_{x2} represents the volume fraction of the mixture. "Abs" is the absorption of the sample. The thermo-optic coefficient of the mixture can be obtained by differentiating the refractive index with temperature. The thermo-optic coefficient of the mixture is given by

$$\frac{dn}{dt} = \frac{3}{2(2L + 1)^{1/2}(1 - L)^{3/2}}\left(\frac{dL}{dT}\right) \tag{18}$$

$$\frac{dL}{dT} = \sum_{i=1}^{2} L_i x_i \tag{19}$$

$$L_i = \left[\frac{\rho}{\rho_i}\left(\frac{d}{dT}\left(\frac{n_i^2 - 1}{n_i^2 + 2}\right)\right) + \left(\frac{n_i^2 - 1}{n_i^2 + 2}\right)\left(\frac{d}{dT}\left(\frac{\rho}{\rho_i}\right)\right)\right], \quad i = 1, 2$$

$$L_i = \frac{\rho}{\rho_i(n_i^2 + 2)}\left[2n_i\left(\frac{dn_i}{dT}\right)\left(1 - \frac{n_i^2 - 1}{n_i^2 + 2}\right) + (n_i^2 - 1)(\beta - \beta_i)\right] \tag{20}$$

In eq 20, the change in density with temperature at constant pressure has been replaced with the product of the density (ρ) and the coefficient of thermal expansion (β) of the solution as well as the corresponding $\beta_i\rho_i$ of the two components of the binary mixtures. Using this phenomenological model, we calculate the various physical parameters and TL signal for all our binary solutions under ideal theoretical conditions. The variation in refractive index with concentration (dn/dc) is simply calculated by differentiating the refractive index of the mixture with the mass fraction of butanol isomers obtained from eq 15. The data obtained from TL experiment is corrected with a fourth order polynomial (Figure 5A) for MeOH and *n*-BuOH binary liquids mixture series as representative case. The corrected data for all four series of binary mixture is shown in Figure 5B.

The absorbance "Abs" calculated from eq 17 is plotted in Figure 6 with the experimentally measured absorbance of

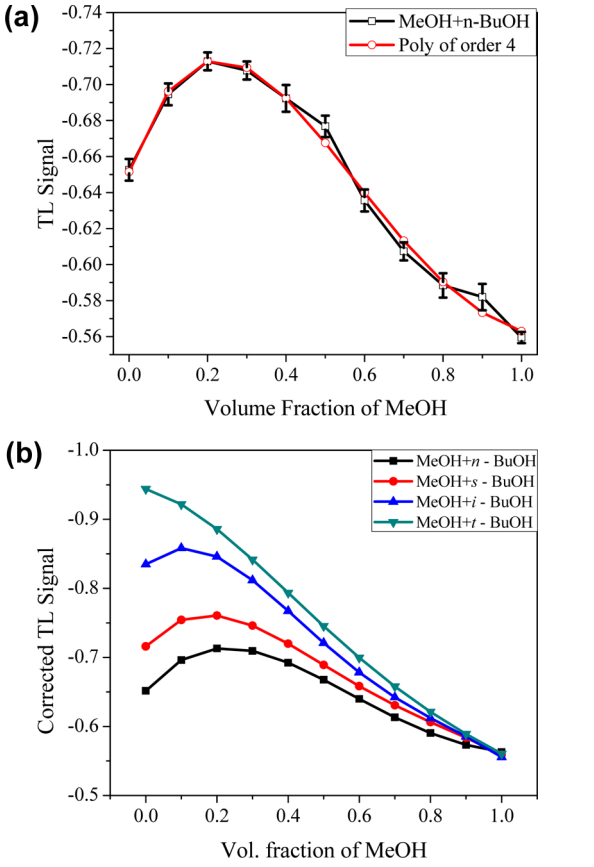

Figure 5. (A) Representative plot of the experimental TL data with respect to volume fraction of MeOH for the MeOH + *n*-BuOH binary mixture and its fit to a fourth order polynomial. (B) Plot of the corrected TL data with respect to volume fraction of MeOH obtained by fourth order polynomial fit to the experimental data for all binary mixtures studied.

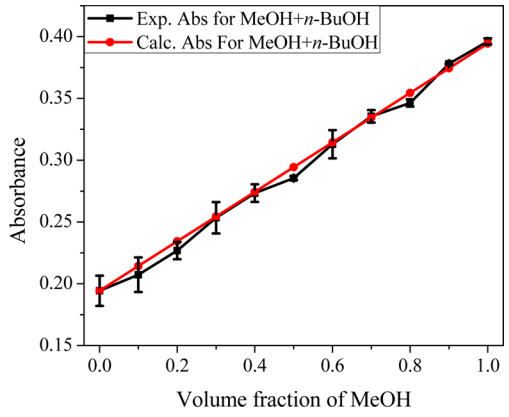

Figure 6. Comparison between the experimentally measured and the theoretically calculated absorbance for MeOH and *n*-BuOH (as a representative case).

MeOH and *n*-BuOH binary liquid mixture series as a representative case. The experimentally measured absorbance of the series is in good agreement with the theoretically calculated ones. The thermal contribution to the total TL signal is calculated from the described physical parameters. The contribution of the concentration gradient to the total thermal lens is calculated from eq 9, and TL contribution of the concentration gradient is shown in Figure 7. Here, it is

dx.doi.org/10.1021/jp5079604 | J. Phys. Chem. B 2014, 118, 14852−14859

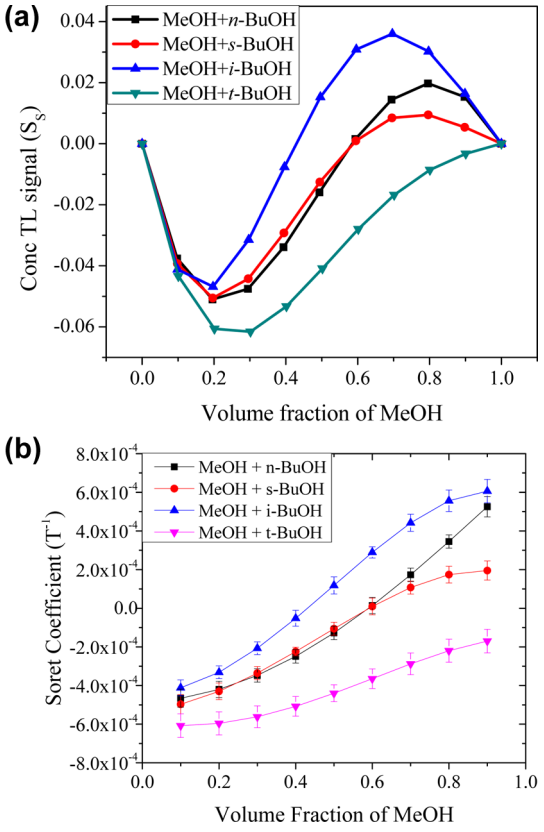

Figure 7. (A) The contribution of concentration gradient TL signal to the total TL signal for all binary liquids mixtures series, namely, MeOH + *n*-BuOH, MeOH + *s*-BuOH, MeOH + *i*-BuOH, and MeOH + *t*-BuOH. (B) Variation of Soret coefficient for the binary liquids mixture series of MeOH with isomers of butanol, namely, MeOH + *n*-BuOH, MeOH + *s*-BuOH, MeOH + *i*-BuOH, and MeOH + *t*-BuOH.

interesting that the contribution of the concentration gradient TL signal to the total TL signal strongly depends on the molecular structure. The concentration TL signal changes its sign from negative to positive with the volume fraction of MeOH for all the isomers of butanol in the binary mixture series except for *t*-BuOH. In the case of the *t*-BuOH binary mixture with MeOH, the concentration TL signal has a negative sign across the concentration of MeOH. The Soret coefficients for the four isomers in the binary mixtures is also calculated by calculating the phase change from eq 7 and 10. The trend in the Soret coefficients for all the butanol series is shown in Figure 7B. In this study, we are able to measure Soret coefficients as low as 10^{-4} K^{-1}. The Soret coefficient has also changed its sign for three isomers of butanol namely, MeOH + *n*-BuOH, MeOH + *s*-BuOH, MeOH + *i*-BuOH. However, the Soret coefficient for MeOH + *t*-BuOH series remain negative throughout the concentration changes in MeOH. The magnitude and the change of sign for Soret coefficient strongly depends on the molecular structure.

CONCLUSION

The Soret effect was assumed to be a mass-driven process that developed when a mixture of two components was subjected to a temperature gradient. Most of the earlier work on the Soret effect was done on mixtures of two components with different masses. We have shown here that even for molecules with the same mass, their structure has a strong effect on the Soret phenomenon. The effect of molecular structure on the Soret phenomenon, possibly due to the diffusion of the molecular isomers, is different under the thermal gradient. The convection time constant (t_d) is smaller for *n*-BuOH and the highest for the *t*-BuOH. The molecular branching makes the system sluggish, and molecular drift becomes progressively difficult as in case of *t*-BuOH. This effect of molecular diffusion is reflected in the Soret coefficient. The Soret coefficient changes its sign across the series of MeOH + *n*-BuOH, MeOH + *s*-BuOH, MeOH + *i*-BuOH. The change of sign in this series has also taken place at different compositions of the two components of the binary liquids mixtures, while the Soret coefficient for the series MeOH + *t*-BuOH does not change its sign and has a negative magnitude. Thus, our systematic study shows that the Soret effect depends on the molecular structure in addition to the dependence on the molecular mass of the two components.

AUTHOR INFORMATION

Corresponding Author

*E-mail: dgoswami@iitk.ac.in.

Notes

The authors declare no competing financial interest.

ACKNOWLEDGMENTS

D.G. thanks the funding support of ISRO Science Technology Cell, DST and MHRD, Govt. of India. P.K. thanks the SPM graduate student fellowship scheme of the CSIR, India.

REFERENCES

(1) Ludwig, C. Diffusoin Zwischen Ungleich Erwwarmten Orten Gleich Zusammengestzter Losungen. *Sitzungsber. Math.-Naturwiss. Kl. Kais. Akad. Wiss.* **1856**, *20*, 539.

(2) Soret, C. Sur l'état d'équilibre que prend au point de vue de sa concentration une dissolution saline primitivement homohéne dont deux parties sont portées a des temperaturés différentes. *Arch. Sci. Phys. Nat.* **1879**, *2*, 46−61.

(3) Srinivasan, S.; Z. Saghir *Thermodiffusion in Multicomponent Mixtures: Thermodynamic, Algebraic, and Neuro-Computing Models*; Springer: London, 2012.

(4) Cabrera, H.; Martí-López, L.; Sira, E.; Rahn, K.; García-Sucre, M. Thermal Lens Measurement of the Soret Coefficient in Acetone/Water Mixtures. *J. Chem. Phys.* **2009**, *131*, 031106.

(5) Kita, R.; Wiegand, S.; Luettmer-Strathmann, J. Sign Change of the Soret Coefficient of Poly(ethylene oxide) in Water/Ethanol Mixtures Observed by Thermal Diffusion Forced Rayleigh Scattering. *J. Chem. Phys.* **2004**, *121*, 3874−3885.

(6) Janca, J. Polarization, Steric, and Focusing Micro-Thermal Field-Flow Fractionation Principles, Theory, Instrumentation, and Applications in Polymers and Particles Analysis. *Anal. Chim. Acta* **2005**, *540*, 187−196.

(7) KiJhler, W.; Rosenauer, C.; Rossmanith, P. Holographic Grating Study of Mass and Thermal-Diffusion of Polystyrene/Toluene Solutions. *Int. J. Thermophys.* **1995**, *16*, 11−21.

(8) Huang, F.; Chakraborty, P.; Lundstrom, C. C.; Holmden, C.; Glessner, J. J. G.; Kieffer, S. W.; Lesher, C. E. Isotope Fractionation in Silicate Melts by Thermal Diffusion. *Nature* **2010**, *464*, 396−401.

(9) Kyser, T. K.; Lesher, C. E.; Walker, D. The Effects of Liquid Immiscibility and Thermal Diffusion on Oxygen Isotopes in Silicate Liquids. *Contrib. Mineral Petrol.* **1998**, *133*, 373−381.

(10) Mast, C. B.; Braun, D. Thermal Trap for DNA Replication. *Phys. Rev. Lett.* **2010**, *104*, 188102.

(11) Obermayer, B.; Krammer, H.; Braun, D.; Gerland, U. Emergence of Information Transmission in a Prebiotic RNA Reactor. *Phys. Rev. Lett.* **2011**, *107*, 018101.

(12) Baaske, P.; Weinert, F. M.; Duhr, S.; Lemke, K. H.; Russell, M. J.; Braun, D. Extreme Accumulation of Nucleotides in Simulated

Hydrothermal Pore Systems. *Proc. Natl. Acad. Sci. U.S.A.* **2007**, *104*, 9346−9351.
(13) Ying, A.; Liu, H.; Abdou, M. Analysis of Tritium/Deuterium Retention and Permeation in FW/Divertor Including Geometric and Temperature Operating Features. *Fusion Sci. Technol.* **2013**, *64*, 303−308.
(14) Morozov, M.; Oron, A.; Nepomnyashchy, A. A. Nonlinear Dynamics of Long-Wave Marangoni Convection in a Binary Mixture with the Soret Effect. *Phys. Fluids* **2013**, *25*, 052107.
(15) Würger, A. Is Soret Equilibrium a Non-Equilibrium Effect? *C. R. Mec.* **2013**, *341*, 438−448.
(16) Jawad, H.; Bataller, H.; Saghir, M. Z. Thermodiffusion Effect for a Non-Associating Mixture in a Multi Layered System of Porous Media and Fluid Layers Heated from Above. *Can. J. Chem. Engg* **2013**, *91*, 1702−1710.
(17) Braun, D.; Libchaber, A. Thermal Force Approach to Molecular Evolution. *Phys. Biol.* **2004**, *1*, 1−8.
(18) Skarabot, M.; Lokar, Z.; Musevic, I. Transport of Particles by a Thermally Induced Gradient of the Order Parameter in Nematic Liquid Crystals. *Phys. Rev. E* **2013**, *87*, 062501.
(19) Yu, W. F.; Lin, Z. Z.; Ning, X. J. Mass Dependence of the Soret Coefficient for Atomic Diffusion in Condensed Matter. *Phys. Rev. E* **2013**, *87*, 062311.
(20) Polyakov, P.; Wiegand, S. Investigation of the Soret Effect in Aqueous and Non-Aqueous Mixtures by the Thermal Lens Technique. *Phys. Chem. Chem. Phys.* **2009**, *11*, 864−871.
(21) Arnaud, N.; Georges, J. cw-Laser Thermal Lens Spectrometry in Binary Mixtures of Water and Organic Solvents: Composition Dependence of the Steady-State and Time-Resolved Signals. *Spectrochim. Acta, Part A* **2004**, *60*, 1817−1823.
(22) Malacarne, L. C.; Astrath, N. G. C.; Medina, A. N.; Herculano, L. S.; Baesso, M. L.; Pedreira, P. R. B.; Shen, J.; Wen, Q.; Michaelian, K. H.; Fairbridge, C. Soret Effect and Photochemical Reaction in Liquids with Laser-Induced Local Heating. *Opt. Exp.* **2011**, *19*, 4047−4058.
(23) Arnaud, N.; Georges, J. Investigation of the Thermal Lens Effect in Water-Ethanol Mixtures: Composition Dependence of the Refractive Index Gradient, the Enhancement Factor and the Soret Effect. *Spectrochim. Acta, Part A* **2001**, *57*, 1295−1301.
(24) Cabrera, H.; Sira, E.; Rahn, K.; García-Sucre, M. A Thermal Lens Model Including the Soret Effect. *Appl. Phys. Lett.* **2009**, *94*, 051103.
(25) Georges, J. Investigation of the Diffusion Coefficient of Polymers and Micelles in Aqueous Solutions Using the Soret Effect in CW-Laser Thermal Lens Spectrometry. *Spectrochim. Acta, Part A* **2003**, *59*, 519−524.
(26) Cabrera, H.; Martí-López, L.; Sira, E.; Rahn, K.; García-Sucre, M. Thermal Lens Measurement of the Soret Coefficient in Acetone/Water Mixtures. *J. Chem. Phys.* **2009**, *131*, 031106.
(27) Santhi, A.; Kala, U. L.; Nedumpara, R. J.; Kurian, A.; Kurup, M. R. P.; Radhakrishnan, P.; Nampoori, V. P. N. Thermal Lens Technique to Evaluate the Fluorescence Quantum Yield of a Schiff Base. *Appl. Phys. B: Laser Opt.* **2004**, *79*, 629−633.
(28) Bhattacharyya, I.; Kumar, P.; Goswami, D. Probing Intermolecular Interaction through Thermal-Lens Spectroscopy. *J. Phys. Chem. B* **2011**, *115*, 262−268.
(29) Bhattacharyya, I.; Priyadarshi, S.; Goswami, D. Molecular Structure-Property Correlations from Optical Nonlinearity and Thermal-Relaxation Dynamics. *Chem. Phys. Lett.* **2009**, *469*, 104−109.
(30) Marcano, A.; Loper, C.; Melikechi, N. Pump−Probe Mode-Mismatched Thermal-Lens Z Scan. *J. Opt. Soc. Am. B* **2002**, *19*, 119−124.
(31) Kumar, P.; Dinda, S.; Chakrabortya, A.; Goswami, D. Unusual Behavior of Thermal Lens in Alcohols. *Phys. Chem. Chem. Phys.* **2014**, *16*, 12291−8.
(32) Bhattacharyya, I.; Kumar, P.; Goswami, D. Effect of Isotope Substitution in Binary Liquids with Thermal-Lens Spectroscopy. *Chem. Phys. Lett.* **2014**, *598*, 35−38.
(33) Sabaeian, M.; Nadgaran, H. An Analytical Model for Finite Radius Dual-Beam Mode-Mismatched Thermal Lens Spectroscopy. *J. Appl. Phys.* **2013**, *114*, 133102.
(34) Viana, J. R. M.; Barboza, M. J.; Rohling, J. H.; Bento, A. C.; Baesso, M. L.; Medina, A. N. Composition Influence on the Thermo-Optical Properties and Luminescence Efficiency of Europium-Doped Calcium Aluminosilicate Glasses. *Int. J. Thermophys.* **2013**, *34*, 1666−1672.
(35) Herculano, L. S.; Malacarne, L. C.; Zanuto, V. S.; Lukasievicz, G. V. B.; Capeloto, O. A.; Astrath, N. G. C. Investigation of the Photobleaching Process of Eosin Y in Aqueous Solution by Thermal Lens Spectroscopy. *J. Phys. Chem. B* **2013**, *117*, 1932−1937.
(36) Ventura, M.; Simionatto, E.; Andrade, L. H. C.; Simionatto, E. L.; Riva, D.; Lima, S. M. The Use of Thermal Lens Spectroscopy to Assess Oil−Biodiesel Blends. *Fuel* **2013**, *103*, 506−511.
(37) Moreira, L. M.; Carvalho, E. A.; Bell, M. J. V.; Anjos, V.; Sant'Ana, A. C.; Alves, A. P. P.; Fragneaud, B.; Sena, L. A.; Archanjo, B. S.; Achete, C. A. Thermo-Optical Properties of Silver and Gold Nanofluids. *J. Therm. Anal. Calorim.* **2013**, *114*, 557−564.
(38) Estupiñán-López, C.; Dominguez, C. T.; Araujo, R. E. D. Eclipsing Thermal Lens Spectroscopy for Fluorescence Quantum Yield Measurement. *Opt. Exp.* **2013**, *21*, 18592.
(39) Saavedra, R.; Soto, C.; Gómez, R.; Muñoz, A. Determination of Lead(II) by Thermal Lens Spectroscopy (TLS) Using 2-(2′-Thiazolylazo)-*p*-cresol (TAC) as Chromophore Reagent. *Microchem. J.* **2013**, *110*, 308−313.
(40) Navea, J. G.; Lopez-Calvo, A.; Manzanares, C. E. Thermal Lens Spectroscopy in Liquid Argon Solutions: ($\Delta\nu$ = 6) C−H Vibrational Overtone Absorption of Methane. *J. Phys. Chem. A* **2006**, *110*, 1594−1599.
(41) Bialkowski, S. E. *Photothermal Spectroscopy Methods for Chemical Analysis*; Wiley: New York, 1996.
(42) Cabrera, H.; Cordido, F.; Velásquez, A.; Morenoa, P.; Sira, E.; López-Rivera, S. A. Measurement of the Soret Coefficients in Organic/Water Mixtures by Thermal Lens Spectrometry. *C. R. Mec.* **2013**, *341*, 372−377.
(43) Andrade, A. A.; Lourenço, S. A.; Pilla, V.; Silvac, A. C. A.; Dantas, N. O. Evidence of Phase Transition in Nd^{3+} Doped Phosphate Glass Determined by Thermal Lens Spectrometry. *Phys. Chem. Chem. Phys.* **2014**, *16*, 1583−9.
(44) Figueiredo, M. S.; Santos, F. A.; Yukimitu, K.; Moraes, J. C. S.; Silva, J. R.; Baesso, M. L.; Nunes, L. A. O.; Andrade, L. H. C.; Lima, S. M. Luminescence Quantum Efficiency at 1.5 μm of Er^{3+}-Doped Tellurite Glass Determined by Thermal Lens Spectroscopy. *Opt. Mater.* **2013**, *35*, 2400−2404.
(45) Gordon, J. P.; Leite, R. C. C.; Moore, R. S.; Porto, S. P. S.; Whinnery, J. R. Long-Transient Effects in Lasers with Inserted Liquid Samples. *J. Appl. Phys.* **1965**, *36*, 3−8.
(46) Sheldon, S. J.; Knight, L. V.; Thorne, J. M. Laser-Induced Thermal Lens Effect: A New Theoretical Model. *Appl. Opt.* **1982**, *21*, 1663−1669.
(47) Shen, J.; Lowe, R. D.; Snook, R. D. A Model for CW Laser Induced Mode-Mismatched Dual-Beam Thermal Lens Spectrometry. *Chem. Phys.* **1992**, *165*, 385−396.
(48) Marcano, A.; Loper, C.; Melikechi, N. Pump−Probe Mode-Mismatched Thermal-Lens Z Scan. *J. Opt. Soc. Am. B* **2002**, *19*, 119−124.
(49) Astrath, N. G. C.; Astrath, F. B. G.; Shen, J.; Zhou, J.; Michaelian, K. H.; Fairbridge, C.; Malacarne, L. C.; Pedreira, P. R. B.; Medina, A. N.; Baesso, M. L. Thermal-Lens Study of Photochemical Reaction Kinetics. *Opt. Lett.* **2009**, *34*, 3460−3462.
(50) Pedreira, P. R. B.; Hirsch, L. R.; Pereira, J. R. D.; Medina, A. N.; Bento, A. C.; Baesso, M. L.; Rollemberg, M. C.; Franko, M.; Shen, J. Real-Time Quantitative Investigation of Photochemical Reaction Using Thermal Lens Measurements: Theory and Experiment. *J. Appl. Phys.* **2006**, *100*, 044906−7.
(51) Astrath, N. G. C.; Astrath, F. B. G.; Shen, J.; Zhou, J.; Michaelian, K. H.; Fairbridge, C.; Malacarne, L. C.; Pedreira, P. R. B.; Santoro, P. A.; Baesso, M. L. Arrhenius Behavior of Hydrocarbon Fuel

Photochemical Reaction Rates by Thermal Lens Spectroscopy. *Appl. Phys. Lett.* **2009**, *95*, 191902−3.
(52) Mian, S. M.; McGee, S. B.; Melikechi, N. Experimental and Theoretical Investigation of Thermal Lensing Effects in Mode-Locked Femtosecond Z-Scan Experiments. *Opt. Commun.* **2002**, *207*, 339−345.
(53) Polyakov, P.; Rossinsky, E.; Wiegand, S. Study of the Soret Effect in Hydrocarbon Chain/Aromatic Compound Mixtures. *J. Phys. Chem. B* **2009**, *113*, 13308.
(54) Kumar, P.; Dinda, S.; Goswami, D. Effect of Molecular Structural Isomers in Thermal Lens Spectroscopy. *Chem. Phys. Lett.* **2014**, *601*, 163−167.
(55) Kumar, P.; Khan, A.; Goswami, D. Importance of Molecular Heat Convection in Time Resolved Thermal Lens Study of Highly Absorbing Samples. *Chem. Phys.* **2014**, *441*, 5−10.
(56) Kauffman, G. W.; Jurs, P. C. Prediction of Surface Tension, Viscosity, and Thermal Conductivity for Common Organic Solvents Using Quantitative Structure−Property Relationships. *J. Chem. Inf. Comput. Sci.* **2001**, *41*, 408−418.
(57) Ortega, J. Densities and Refractive Indices of Pure Alcohols as a Function of Temperature. *J. Chem. Eng. Data* **1982**, *27*, 312−317.
(58) Kijevcanin, M. L.; Radovic, I. R.; Djordjevic, B. D.; Tasic, A. Z.; Serbanovic, S. P. Experimental Determination and Modeling of Densities and Refractive Indices of the Binary Systems Alcohol + Dicyclohexylamine at T = (288.15−323.15) K. *Thermochim. Acta* **2011**, *525*, 114−128.
(59) Riggio, R.; Ramos, J. F.; Ubeda, M. H.; Espindola, J. A. Mixtures of Methyl Isobutyl Ketone with Three Butanols at Various Temperatures. *Can. J. Chem.* **1981**, *59*, 3305−3308.